A new modelling framework for sea ice mechanics based on elasto-brittle rheology

Lucas GIRARD,[1] Sylvain BOUILLON,[3] Jérôme WEISS,[1] David AMITRANO,[2] Vincent LEGAT,[3]

[1] *Laboratoire de Glaciologie et de Géophysique de l'Environnement, CNRS - Université Joseph Fourier, Grenoble, France*
E-mail: lgirard@lgge.obs.ujf-grenoble.fr
[2] *Laboratoire de Géophysique Interne et de Tectonophysique, CNRS - Université Joseph Fourier, Grenoble, France*
[3] *Université catholique de Louvain, Louvain-la-Neuve, Belgium*

ABSTRACT. We present a new and original modelling framework for sea ice mechanics based on elasto-brittle (EB) behavior. The EB framework considers sea ice as a continuous elastic plate encountering progressive damage, reflecting the opening of cracks and leads. As the result of long-range elastic interactions, the stress relaxation following a damage event can induce an avalanche of damage. Damage propagates in narrow linear features, resulting in a very heterogeneous strain field. Idealized simulations of the Arctic sea ice cover are analysed in terms of ice deformation and contrasted to observations and simulations performed with the Viscous Plastic (VP) rheology. We show that the EB simulations give a good representation of the shear faulting mechanism that accomodates most of sea ice deformation. The distributions of strain-rates and the scaling law of ice deformation are well captured by the EB framework, which is not the case for VP simulations. These results argue that the properties of ice deformation emerge from the ice mechanical behavior and motivate the implementation of the EB framework in a global sea ice model.

1. INTRODUCTION

Sea ice deformation is a fascinating component of the Arctic geophysical environnement which is of critical importance in climate modelling. The deformation of dense pack ice is accomodated by a network of quasi-linear fractures and faults, occuring over a wide range of scales, up to several hundred kilometers, resulting in an heterogenous and intermittent strain field (Weiss and others, 2007; Marsan and others, 2004; Rampal and others, 2008; Stern and Lindsay, 2009). Opening of new leads in the sea ice cover is a source of rapid heat exchanges between the ocean and the atmosphere, new ice growth and brine rejection to the ocean. Seasonal ice growth in fractures accounts for 25 to 40% of the total ice production of the Arctic ocean (Kwok, 2006). For these reasons, global climate models all include a relatively sophisticated description of the dynamics and thermodynamics of the sea ice cover. These models should therefore be able to capture the properties of sea ice deformation.

Sea ice rheology describes the relationship between the ice stress (or internal ice forces), the deformation of the ice cover and the material properties of sea ice. The determination of suitable constitutive relations to describe sea ice rheology has guided sea ice-dynamics research since it began, and it remains an outstanding problem that limits the success of sea ice models (Feltham, 2008). Most sea ice models currently used in climate models stem from the seminal work of Hibler (1979) who described the ice cover in terms of viscous-plastic (VP) mechanics associated with a rate- and scale-independent failure envelope. This modelling framework, based on a fluid-like mechanics approach, where ice flows either as a Newtonian fluid or pastically, is not suited to describe the multiscale fracturing processes that accomodate sea ice deformation. As show below, the main drawback of this framework is that it does not consider long-range elastic interactions which are at the root of strain localization, intermittency and scaling.

In the Arctic, two major datasets can be used to evaluate sea ice models in terms of ice deformation. Strain-rates can be derived from drifting buoy trajectories (Rampal and others, 2008) or from the sea ice kinematics produced by the RADARSAT Geophysical Processor System (RGPS) (Kwok, 1998) which provides strain-rate estimates down to 10km spatial scale at a near basin-scale context. Based on comparisons with these two datasets, poor correlations between the deformation rates simulated by the VP rheology and observations have been reported from regional scales ($\sim$ 300km) to small scales ($\sim$ 10km) (Thomas, 1999; Lindsay and others, 2003; Kwok and others, 2008).

However, the main difficulty for the evaluation of sea ice rheological models is the definition of an appropriate metric. A high correlation between model and observed ice deformation is desirable, but it cannot be expected at small spatial and temporal scales (e.g. $<$ 100km and $<$ 1 month), since sea ice velocity is mostly stochastic at such scales (Rampal and others, 2009). Correlation coefficients are thus not the best metric to evaluate models. On the other hand, sea ice deformation exhibits specific statistical and scaling properties that provide an alternative validation metric as they are the signature of the underlying fracturing and faulting processes.

These properties are expressed by a power law scaling of ice strain-rate, a relationship of the form $< \dot{\epsilon} >= a.L^{-b}$, that relates the mean deformation rate to the spatial scale L over which it is measured, a and b being constants. The scaling relationship has been extensively analyzed from buoys observations (Rampal and others, 2008) and RGPS observations (Stern and Lindsay, 2009). It also extends to the other moments of the strain-rate, $< \dot{\epsilon}^q > \sim L^{-b(q)}$, expressing the

dependance of the strain-rate distribution upon the spatial scale of observation (Marsan and others, 2004).

Girard and others (2009) applied this validation metric to high resolution coupled ocean/sea ice simulations performed with the VP rheology and Elasto-viscous-plastic (EVP) derivative. These authors showed that the statistical properties characterizing sea ice deformation were not reproduced by the simulations, even at large spatial scales. As these properties emanate from the ice mechanical behavior (Weiss, 2008; Rampal and others, 2009) this suggests that the mechanical framework of the VP rheology is inapropriate.

The aim of this paper is to introduce a new mechanical framework for sea ice modelling based on an elasto-brittle (EB) constitutive law. This framework is intended to be able to reproduce the statistical and scaling properties that characterize sea ice deformation. It is based on continuum mechanics and is simple enough to be implemented in climate models. The main characteristics of the rheology are progressive damage, which reflects how cracks and faults affect the ice mechanical properties, and long range elastic interactions. Basin-scale simulations over short time scales (72 h) are performed with an idealized finite element application of the model at 10 km resolution. The simulations presented are only forced by wind stress and focus specifically on resulting sea ice deformation, the thermodynamics and the advection of ice are not considered here. We show that heterogeneous deformation fields are obtained with the EB rheology and that complexity arises from elastic interactions on a wide range of scales.

For comparison purposes, simulations with similar setup and forcing are performed with the VP rheology. Observations of sea ice deformation from the RGPS database are also considered. The statistical and scaling properties of ice deformation are used as the validation metric. We show that the EB rheology gives a much better representation of these properties than the VP rheology.

2. MODELS AND OBSERVATIONS

2.1. EB mechanical framework

The EB framework is built on continuum mechanics in order to be suitable for inclusion within a regional or global climate model. The physics accounts for the fracturing processes occuring in the sea ice cover and the elastic interactions that can propagate on long distances, following the arguments of Weiss and others (2007). Fracturing processes are considered to play an essential role for sea ice deformation and dynamics (Weiss and others, 2009; Marsan and others, 2004; Schulson, 2004; Schulson and Hibler, 1991). In the EB model, sea ice is considered as a continuous $2D$ elastic plate. The ice thickness is not considered explicitely. It is however taken into account in the formulation of the elastic stiffness (see eq. 4). The effect of fracturing is represented through progressive damage, expressed by a reduction of the local/grid-scale elastic stiffness,

$$K = K_0 \times d \tag{1}$$

where K and K_0 are respectively the effective and initial elastic stiffnesses and $d \leq 1$ is a scalar indicating the damage level (Kachanov, 1986). This formulation implies that the effect of sub-grid scale fracturing is represented by a scalar damage level at the grid scale. The damage level thus reflects the density of cracks and leads within the ice cover. A similar framework was used in theoretical studies investigating the statistical properties of fracture in brittle materials (Girard and others, 2010; Amitrano and others, 1999).

The mechanical framework is applied to an idealized model of the Arctic sea ice cover using a finite element method with plane-stress hypothesis, continuous and linear discretization. The model considers a quasi-static ice cover (no advection) driven by wind stress. This simplified application aims at investigating the ice response, in terms of deformation, to the wind forcing on short time scales (3 days). The other terms of the momentum balance are neglected in this study as the geostrophic wind is thought to explain more than 70% of the variance of the sea ice velocity in the central Arctic Ocean on short time scales (Thorndike and Colony, 1982). The ice thickness h and concentration c which determine the initial elastic properties (eq. 4) are initialized at the beginning of simulations and considered to be constant throughout the simulations. For the time scale considered, ice advection and thickness variations are assumed neglegible. With these assumptions, the momentum balance simply reads (forces per unit area),

$$\nabla . \underline{\underline{\sigma}} = \underline{\tau_a} \tag{2}$$

where $\underline{\underline{\sigma}}$ is the ice internal stress tensor and $\underline{\tau_a}$ is the wind stress, calculated with an air turning angle of zero as we use 10-m wind fields (McPhee, 1975),

$$\underline{\tau_a} = \rho_a \times C_a \times \left\|\underline{u_a}\right\| \times \underline{u_a} \tag{3}$$

where ρ_a is the air density, C_a the air drag coefficient and $\underline{u_a}$ the wind velocity. The undamaged elastic stiffness of the ice K_0 is expressed as a function of a Young modulus Y, the ice thickness h, the ice concentration c and a constant ν following the parameterisation used for the ice strength in VP models (see eq. 16),

$$K_0 = Y \times h \times exp^{-\nu(1-c)} \tag{4}$$

At each model step, when the stress of an element, i, exceeds a given strength threshold for damage, its elastic stiffness K_i is multiplied by a constant damage factor $d_0 = 0.9$,

$$K_i(n+1) = K_i(n) \times d_0 \tag{5}$$

n being the number of damage events of the element i. After n damage events the effective stiffness, $K_i(n)$ is given by,

$$K_i(n) = K_{i,0} \times d_0^n \tag{6}$$

where $K_{i,0}$ is the undamaged elastic stiffness. After each damage event, the state equilibrium is calculated to redistribute stresses within the elastic plate. Because of the elastic interactions, the stress redistribution around a damaged element can induce damage on neighboring elements and onset an avalanche of damaged elements which may propagate on long distances across the ice cover. The avalanche stops when the damage criterion is no more fulfilled by any element, setting the end of the time step. Stress redistribution and the induced damage propagation are key ingredients of this new EB framework and constitute a major difference with former fluid-like frameworks.

In-situ stress measurements (Weiss and others, 2007) and laboratory experiments (Schulson and others, 2006) both argue in favor of Coulombic faulting within the sea ice cover. We therefore choose the Coulomb criterion to define the damage threshold,

$$\tau = \mu\sigma_N + C \tag{7}$$

where τ and σ_N are respectively the shear and the normal stress at the scale of the element, C is the cohesion and μ

is the internal friction coefficient. The internal friction coefficient is set to $\mu = 0.7$. This is in the range of values measured by Fortt and Schulson (2007) from sliding experiments along Coulombic shear faults in laboratory-grown freshwater ice. It is also relevant at geophysical scales for sea ice with a similar internal friction coefficient (Weiss and Schulson, 2009). To simulate material heterogeneity, which consists in defaults and cracks in the ice at sub-grid scales, the value of the cohesion C is randomly drawn from a uniform distribution. In the simulations, we arbitrarily set the C-range between 10 to 20 kPa. This range is close to the values estimated from in-situ stress measurements with values of about 40 kPa for the cohesion (Weiss and others, 2007). As suggested by observations, we apply a tensile strength threshold to the criterion for $\sigma_N = -40$ kPa (the sign convention chosen is negative for tension).

Field measurements of the sea ice Young modulus report values between 7 and 10 GPa depending on the volume fraction of brines and the porosity (Schulson and Duval, 2009). Such value applies for the bulk material, it is related to the measurement scale (cm to m) and performed on crack-free samples. Our model application requires an apparent Young modulus Y associated with the grid scale, 10 km in this study. This apparent Young modulus will be much smaller than the bulk modulus due to the existence of cracks and faults at sub-grid scales. A decrease in apparent Young modulus leads to larger mean ice deformation.

We perform sensitivity tests to determine the apparent Young modulus at each model resolution which leads to a simulated mean total deformation at the grid scale comparable to the value estimated by RGPS observations. At 10 km and a temporal scale of 3 days, in March, this value is typically $< \dot{\epsilon}_{tot} >= 0.014$ /day (Stern and Lindsay, 2009). The methodology is applied to all simulations and the results are averaged over the different time periods simulated, leading to $Y = 500$ Mpa. This value should only be taken as an order of magnitude as the simulations only cover short periods of time. The physical parameter and constants used in this study are summarized in table 1.

2.2. Simulations setup

The simulations are performed on a mesh composed of triangular elements covering the oceans from 50°N up to the North Pole. The effective resolution of mesh is 10 km, below 65°N the resolution coarsens to 150 km.

The ice thickness and concentration are initialized from a reference simulation ($ORCA025 - G70$) obtained with the global coupled ocean model Drakkar (Barnier and others, 2006). It is forced by ECMWF products. The simulations hindcasts compare well with observations in terms of ice extent and concentration (Drakkar-Group, 2007). The ice thickness and concentration obtained from this Drakkar simulation for 2007-March-1 are interpolated to the mesh and used as the initial conditions of our simulations (figure 1). No-slip boundary condition is imposed on the coast.

The wind speed used to drive the simulations is obtained from the 6-hourly ECMWF operational analyses (10-m wind speed), with an effective resolution of ~ 80 km in the central Arctic. The wind speed is linearly interpolated in space and time at every model step. The total duration of the simulations is 96 hours. During the first 24 h, considered as a spin-up, the wind stress is progressively increased up to its nominal value, which is then applied during the rest of the simulation (72 h). The time step used in all simulations is 20 seconds. Simulations are performed over three time periods starting on March 15^{th},19^{th} and 27^{th} 2007.

2.3. VP simulations

The VP model used for the comparison with EB is based on the work of Lietaer and others (2008). The ice momentum equation for VP simulations has been simplified to be almost similar to the one used for EB simulations,

$$\underline{\tau_a} + \underline{\tau_w} - \nabla.\underline{\underline{\sigma}} = 0 \tag{8}$$

where $\underline{\underline{\sigma}}$ is the ice internal stress tensor given by the VP rheology, $\underline{\tau_a}$ is the same wind stress as for EB rheology and $\underline{\tau_w}$ is the water drag term for an ocean at rest and is given by the following expression :

$$\underline{\tau_w} = -\rho_w C_w \left\|\underline{u}\right\| \underline{u} \tag{9}$$

where ρ_w is the water density, C_w the water drag coefficient and $\underline{u}$ the ice velocity.

The $\underline{\underline{\sigma}}$ tensor is defined as a function of the deformation rate tensor $\underline{\underline{\dot{\epsilon}}}$ and two of its invariants, the divergence rate $\dot{\epsilon}_{div}$ and the shear rate $\dot{\epsilon}_{shear}$:

$$\underline{\underline{\dot{\epsilon}}} = \frac{1}{2}\left(\nabla\underline{u} + \nabla\underline{u}^T\right) \tag{10}$$

$$\dot{\epsilon}_{div} = \dot{\epsilon}_{11} + \dot{\epsilon}_{22} \tag{11}$$

$$\dot{\epsilon}_{shear} = \sqrt{\left(\dot{\epsilon}_{11} - \dot{\epsilon}_{22}\right)^2 + \left(\dot{\epsilon}_{12} + \dot{\epsilon}_{21}\right)^2}. \tag{12}$$

The VP rheology simulates the plastic behavior with the following equations :

$$\underline{\underline{\sigma}} = 2\eta\underline{\underline{\dot{\epsilon}}} + \left((\zeta - \eta)\dot{\epsilon}_{ii} - \frac{P}{2}\right)\underline{\underline{I}} \tag{13}$$

$$\zeta = \frac{P}{2\gamma},\ \eta = \frac{\zeta}{e}, \tag{14}$$

$$\gamma = max\left(\sqrt{\dot{\epsilon}_{div}^2 + \frac{1}{e^2}\dot{\epsilon}_{shear}^2}, \gamma_{min}\right). \tag{15}$$

Those equations ensure that if the deformation rate is greater than γ_{min}, the compressive stress, $\sigma_{div} = \sigma_{11} + \sigma_{22}$ and the shearing stress, $\sigma_{shear} = \sqrt{\left(\sigma_{11} - \sigma_{22}\right)^2 + \left(\sigma_{12} + \sigma_{21}\right)^2}$ will define an elliptical yield curve of size P and with an aspect ratio equals to $\frac{1}{e}$. When the deformation rate is smaller than γ_{min}, the ice behaves as a viscous fluid. The ice strength P is parametrized by :

$$P = P^* h\ exp^{-\nu(1-c)}. \tag{16}$$

Simulations with VP rheology are performed with the same setup as the EB numerical experiments. The mesh is the similar but the computation for VP is made on the sphere (Comblen and others, 2008) whereas it is done on a projection on a plane for EB. Ice initial conditions and wind forcings are interpolated from the same datasets. We also used the same parametrization of the wind stress. The timestep is about one hour and viscosities are computed from the deformation rate of the preceding timestep. The finite element discretization is continuous and linear, and the no-slip boundary condition is strongly imposed on the coast.

2.4. RGPS Observations

RGPS observations of ice deformation from March 2007 are used in this study for statistical comparisons with the simulations presented. RGPS is based on a cross-correlation technique applied to consecutive SAR images (Fily and Rothrock, 1990), which allows tracking in a Lagrangian fashion of more than 40,000 points over the Canadian side of the Arctic during

an entire season (http://www-radar.jpl.nasa.gov/rgps/). The tracked points define the corners of cells which are initially squared ($10 \times 10\,\mathrm{km}^2$). The spatial gradients of the velocity field $\partial u/\partial x$, $\partial v/\partial x$, $\partial u/\partial y$, $\partial v/\partial y$ are computed for each of the cell over the period between two observations (sampled at irregular time intervals within the domain, but typically 3 days) (Kwok, 1998). Recast in terms of strain-rate tensor components,

$$\dot{e}_{11} = \partial u/\partial x \tag{17}$$

$$\dot{e}_{22} = \partial v/\partial y \tag{18}$$

$$\dot{e}_{12} = \dot{e}_{21} = (\partial u/\partial y + \partial v/\partial x)/2 \tag{19}$$

The shear and divergence rates can finally be calculated (eq. 11,12) along with the total deformation rate $\dot{\epsilon_{tot}} = \sqrt{\dot{\epsilon}^2_{shear} + \dot{\epsilon}^2_{div}}$. Further details on RGPS observations and their accuracy are presented in Lindsay and Stern (2003).

3. DAMAGE LOCALIZATION IN EB SIMULATIONS

In the early stages of EB simulations, the elastic stiffness of the ice cover, set by ice thickness and concentration fields (figure 1), varies smoothly over the ocean. During spinup the wind stress is progressively increased and damage events start to occur. These damage events are first homogeneously scattered throughout the Arctic ocean. The reduction of elastic stiffness occuring when an element is damaged induces a stress redistribution on the neighbouring elements, which can trigger other damage events and onset an avalanche of damage. Further on in the simulations, large avalanches occur corresponding to the propagation of the stress relaxation over long distances. This results in linear damage bands, which are the expression of long range elastic interactions that take place within the ice cover (figure 2). These linear features represent active faults that concentrate shear deformation and divergence (see below). Most of them are very narrow, as observed for real faults (Schulson, 2004), with a width set by the spatial resolution (i.e. one element wide).

Note that this heterogeneity in the damage field is not originally set as an initial condition in the simulations, instead it emerges from elastic interactions between the elements. This can be illustrated by performing a simulation without reduction of elastic stiffness ($d_0 = 1$). In this case, damage events occur only locally, in places where the wind stress is sufficiently large. Damage remains scattered without localization and linear faults disappear (figure 2).

4. DEFORMATION FIELDS AND LINEAR KINEMATIC FEATURES

Figure 3 shows an example of the shear and divergence rates from EB and VP simulations, calculated for the 3-day period of the simulation. The RGPS observations available for this time period are also plotted. Similar results are obtained for the other time periods considered. The simulated strain-rates are calculated at the grid scale, 10 km, which is also the length scale of the RGPS Lagrangian cells. Considering the high resolution and the idealized settings and forcing, the simulations are definitely not expected to predict the observed ice strain field. Furthermore, our simulations are started with a nearly homogeneous ice cover at rest, while the deformation of the central Arctic ice pack is known to keep 'memory' of large deformation events during the course of a winter season and major faults can be activated several times (Coon and others, 2007). Nevertheless, EB and VP results can be contrasted with each other and with the available observations. The comparison is focused on the central Arctic ocean (150km away from coastlines and straits), since we have simplified the ice momentum equation and considered only the wind forcing.

The deformation fields obtained with the EB rheology show strong localization of the deformation, in agreement with the observations. As an illustration, in RGPS observations the largest 50% of all shear is accomodated by only 6% of the surface area, a value close to that obtained with the EB simulation, 4%. In contrast, the VP strain field is much less localized, with the largest 50% of all shear accomodated by more than 20% of the ice surface. Insights on mechanisms driving the ice deformation can be obtained by analysing the correlations between shear and divergence fields. RGPS observations show a strong correlation between the shear and divergence fields ($R^2 = 0.83$) that argues for a shear faulting mechanism associated with dilatancy (Weiss and Schulson, 2009): shearing along rough faults is necessarily accompagnied by fault opening, i.e. divergence. The correlation between shear and divergence is also high in the EB simulation ($R^2 = 0.77$) but significantly lower in the VP simulation ($R^2 = 0.58$). This shows that the EB modelling framework captures well the physics of shear faulting that accomodates most of sea ice deformation. The mechanical framework is thus able to generate the so-called linear kinematic features with a similar mechanism as the observations.

5. STRAIN-RATE DISTRIBUTIONS

For many climate applications, it is most important to get a good estimate of the strain-rate distributions in models than to obtain a good correlation with observations, since the statistics of the deformation and the shape of distribution functions impacts winter ice growth rates (Lindsay and others, 2003). Furthermore, at small spatial and temporal scales, to predict in a deterministic sense the ice deformation field is impossible considering the stochastic behavior of ice velocity fluctuations at such scales. Simulated strain-rates are thus evaluated against observations through their probability density functions (PDF). The PDF of RGPS strain-rates is known to exhibit a power law decay, $p(\dot{\epsilon}) \sim \dot{\epsilon}^{-\alpha}$, where α depends on the spatial scale considered (Marsan and others, 2004). Such distributions are characterized by 'wild randomness' and dominated by extreme values. The PDF of strain-rates simulated by the VP rheology were showed have a very different shape, without power law behavior. Instead, they are in the Gaussian attraction basin and are associated with 'mild randomness', the extreme values are not captured (Girard and others, 2009).

Figure 4 shows the PDF of shear and absolute divergence rates for EB and VP simulations and RGPS observations. Simulated strain-rates are extracted from all simulations, from the central Arctic ocean (150 km away from the coastlines, the Fram and Bering straits). In order to get a statistically representative amount of observations, all RGPS measurements of March 2007 were considered. The PDF obtained with the observations does not vary significantly if only a part of these data is considered.

The PDF of shear rates obtained with EB simulations compares very well with the RGPS observations, with a clear power law behavior over 3 orders of magnitude with an exponent of 2.2. The fact that these statistical properties are

well captured by the EB simulations is a strong argument in favor of the new mechanical framework. Regarding the PDF of divergence rates, the agreement between observations and the EB rheology is quite good. Both the EB and observed PDFs show a power law decay, with an exponent of 2.5 for the observations and 2.1 for EB simulations.

Our results also confirm the strong discrepancy between the distributions of VP strain-rates and the observations. The EB framework successfully captures the statistical properties of strain-rates and the power law tail of the PDFs, while the VP rheology does not.

6. SCALING PROPERTIES OF ICE DEFORMATION

Sea ice deformation is characterized by spatial as well as temporal scaling laws which are the signature of long-range elastic interactions and space-time coupling (Weiss and others, 2009; Rampal and others, 2008; Marsan and others, 2004). These scaling laws are not inherited from the wind-forcing but emanate from the ice mechanical behavior and thus consitute an interesting metric to evaluate the physics of sea ice models. The spatial scaling of simulated ice deformation is analyzed in this study and compared with the scaling law obtained from observations. Seasonal variations of the spatial scaling have been explored (Stern and Lindsay, 2009), the analysis we perform is intended to be representative of March 2007. Three daily strain-rates obtained from the 3 different time periods of the simulations are thus merged and all RGPS observations from March 2007 are considered for the analysis (a dataset similar to the previous section). A coarse graining procedure is applied to the strain-rates in order to compute the total deformation rates on a wide range of scales (10 km ot 1000 km) following the methodology presented by Marsan and others (2004). Figure 5 shows the mean total deformation rate as a function of the spatial scale.

The observations show a power law scaling of the mean total deformation rate, $< \dot{\epsilon}_{tot} > \sim L^{-b}$, with $b = 0.17$. The last bin shows a small deviation from this power law behavior and could be due to a finite size effect, as the scale reaches the order of magnitude of the width of the Arctic basin. A similar exponent of the scaling law has been reported before for March (Stern and Lindsay, 2009). Regarding the models, the EB simulated deformation fields also show a power law scaling which is characterized by a slightly shallower exponent, $b = 0.1$. The last bin also appears to be affected by a finite size effect. If single EB simulations are considered, the scaling exponent shows variations between $b = 0.09$ and 0.15. This is slightly lower than the range expected for observations in March (roughly $b = 0.12$ to 0.20). On the other hand, the VP simulated strain-rate does not vary significantly with the scale, except a small decrease towards large scales which, once again, is probably the expression of a finite size effect.

The power law scaling obtained for EB simulations is another argument in favor of the new mechanical framework. It expresses the heterogeneity of the simulated deformation field that emerges from elastic interactions between elements over a wide range of scales. The limit at small scales is only fixed by the model resolution. This means that running simulations at higher resolution will result in increased localization of the deformation and involve larger strain-rates.

7. DISCUSSION AND CONCLUSIONS

An elasto-brittle mechanical framework for sea ice models has been presented. This framework is intended to describe the mechanical behavior of dense pack ice, for ice concentrations typically above 80%. In this case, stresses can be transmitted on long distances across the ice cover resulting in heterogeneous deformation fields characterized by specific statistical and scaling properties. These mechanisms are described in the EB framework by progressive damage and long range elastic interactions. The results presented in this study demonstrate that such physics allows the emergence of heterogeneity in the simulated ice deformation. The statistics of ice deformation are well represented by the EB rheology although the simulations considered here are rather crude and consider only short time periods. This is a noteworthy point since no other model of sea ice mechanics had successed in capturing these properties so far. In particular, the VP rheology, currently used in most sea ice model, has been shown to be unable to capture the properties of ice deformation (Lindsay and others, 2003; Girard and others, 2009).

Our results support the scenario proposed by Weiss and others (2007) considering that fracture and frictional sliding govern the inelastic deformation over a wide range of spatial scales. A viewpoint which was also shared in the granular sea ice model of Hopkins and Thorndike (2006). The EB rheology offers the advantage of using continuum mechanics which is more suitable for the implementation in a global coupled ocean-sea ice model. At time scales longer than a few days, the effect refreezing, or 'healing', of damaged areas on ice mechanics needs to be accounted for. By opposition to damage, healing tends to restore the initial ice mechanical properties, when temperature conditions allow refreezing. The healing needs to be implemented before the EB framework can be used in global sea ice models on longer time periods.

A possible justification of the poor quality of the VP simulated ice deformation is the resolution and the representativity of the wind fields used to drive sea ice models, there is now evidence that this argument is not acceptable. The simulations presented in this study are driven by wind fields derived from reanalysis, similarly to global sea ice models, with an effective resolution of about 80 km. In such products boundary layer turbulence and small scale variability of the wind velocity are indeed not captured. Albeit this smooth forcing, EB simulated deformation is heterogeneous and the localization of deformation occurs down to the grid scale, 10 km. This provides an interesting insight on the origin of the statistical and scaling properties of sea ice deformation: they cannot be inherited from the wind forcing since the deformation fields obtained show scaling down to the grid scale, which is much smaller than the wind forcing resolution. This supports the conclusions of Rampal and others (2009) drawn from statistical analysis bouy derived ice deformation. Our results argue that the statistics of sea ice deformation arise from the elasto-brittle mechanical behavior of the ice. In other words, the limitation of current sea ice models, based on the VP rheology is not due to the resolution and the quality of the forcing, but to the model physics itself. Increasing the resolution of VP-based models does not help capturing the properties of ice deformation.

ACKNOWLEDGEMENTS

The RGPS data were provided by the Polar Remote Sensing Group at JPL. ECMWF analyses were provided in the

framework of the Drakkar cooperation on global ocean/sea-ice modelling. We are grateful to the MEOM-LEGI team for providing the Drakkar OGCM simulation. The EB simulations presented in this paper were performed at the Service Commun de Calcul Intensif de l'Observatoire de Grenoble (SCCI-CIMENT). D. Amitrano thanks French program INSU-Catell and EU program Trigs for support. L. Girard is supported by a BDI phD grant from CNRS. P. Rampal is warmly acknowledged for thrilling discussions and encouragements.

REFERENCES

Amitrano, D., J. R. Grasso and D. Hantz, 1999. From diffuse to localised damage through elastic interaction, *Geophys. Res. Lett.*, **26**, 2109 – 2112.

Barnier, B., G. Madec, T. Penduff, J.M. Molines, A.M. Trguier, A. Beckmann, A. Biastoch, C. Boning, J. Dengg, S. Gulev, J. Le Sommer, E. Rmy, C. Talandier, S. Theetten, M. Maltrud and J. Mc Lean, 2006. Impact of partial steps and momentum advection schemes in a global ocean circulation model at eddy permitting resolution, *Ocean Dynamics*, **56**, 543 – 567.

Comblen, R., S. Legrand, E. Deleersnijder and V. Legat, 2008. A finite element method for solving the shallow water equations on the sphere, *Ocean Modelling*, **28**, 12 – 23.

Coon, M., R. Kwok, G. Levy, M. Pruis, H. Schreyer and D. Sulsky, 2007. Arctic ice dynamics joint experiment (AIDJEX) assumptions revisited and found inadequate, *J. Geophys. Res.-Oceans*, **112**(C11S90).

Drakkar-Group, 2007. Eddy-permitting ocean circulation hindcasts of past decades, *CLIVAR Exchanges*, **12**(3).

Feltham, D.L., 2008. Sea ice rheology, *Annual Review of Fluid Mechanics*, **40**, 91 – 112.

Fily, M. and D.A. Rothrock, 1990. Opening and closing of sea ice leads: digital measurements from synthetic aperture radar, *J. Geophys. Res.*, **95**, 789 – 796.

Fortt, A.L. and E.M. Schulson, 2007. The resistance to sliding along Coulombic shear faults in ice, *Acta Materialia*, **55**, 2253 –2264.

Girard, L., D. Amitrano and J. Weiss, 2010. Failure as a critical phenomenon in a progressive damage model, *Journal of Statistical Mechanics: Theory and Experiment*, (P01013).

Girard, L., J. Weiss, J.M. Molines, B. Barnier and S. Bouillon, 2009. Evaluation of high-resolution sea ice models on the basis of statistical and scaling properties of Arctic sea ice drift and deformation, *J. Geophys. Res.*, **114**(C08015).

Hibler, W.D., 1979. A dynamic thermodynamics sea ice model, *J. Phys. Oceanogr.*, **9**, 815 – 846.

Hopkins, M. A. and A. S. Thorndike, 2006. Floe formation in Arctic sea ice, *J. Geophys. Res. Oceans*, **111**(C11S23).

Kachanov, L.M., 1986. Introduction to continuum damage mechanics, Martinus Nijhoff Publishers.

Kwok, R., 1998. The RADARSAT geophysical processor system, in Analysis of SAR data of the polar oceans: Recent Advances, Springer, New York, 235 – 257.

Kwok, R., 2006. Contrasts in sea ice deformation and production in the Arctic seasonal and perennial ice zones, *J. Geophys. Res.*, **111**(C11S22).

Kwok, R., E. C. Hunke, W. Maslowski, D. Menemenlis and J. Zhang, 2008. Variability of sea ice simulations assessed with RGPS kinematics, *J. Geophys. Res.*, **113**(C11012).

Lietaer, O., T. Fichefet and V. Legat, 2008. The effects of resolving the Canadian Arctic Archipelago in a finite element sea ice model, *Ocean Modelling*, **24**, 140 – 152.

Lindsay, R.W. and H.L. Stern, 2003. The RADARSAT geophysical processor system: Quality of sea ice trajectory and deformation estimates, *Journal of Atmospheric and Oceanic Technology*, **20**, 1333 – 1347.

Lindsay, R.W., J. Zhang and D.A. Rothrock, 2003. Sea-ice deformation rates from satellite measurements and in a model, *Atmosphere-Ocean*, **41**, 35 – 47.

Marsan, D., H. Stern, R. Lindsay and J. Weiss, 2004. Scale dependence and localization of the deformation of arctic sea ice, *Phys. Rev. Lett.*, **93**(178501).

McPhee, M.G., 1975. Ice-ocean momentum transfer for the AIDJEX ice model, *AIDJEX Bull.*, **29**, 93 – 111.

Rampal, P., J. Weiss and D. Marsan, 2009. Arctic sea ice velocity field: general circulation and turbulent-like fluctuations, *J. Geophys. Res.*, **114**(C10014).

Rampal, P., J. Weiss, D. Marsan, R. Lindsay and H. Stern, 2008. Scaling properties of sea ice deformation from buoy dispersion analyses, *J. Geophys. Res.*, **113**(C03002).

Schulson, E.M., 2004. Compressive shear faults within the arctic sea ice: fracture on scales large and small, *J. Geophys. Res.*, **109**(C07016).

Schulson, E.M., A.L. Fortt, D. Iliescu and C.E. Renshaw, 2006. Failure envelope of first-year Arctic sea ice: The role of friction in compressive fracture, *J. Geophys. Res.*, **111**(C11S25).

Schulson, E.M. and W.D. Hibler, 1991. The fracture of ice on scales large and small: arctic leads and wing cracks, *J. Glaciol.*, **37**, 319 – 322.

Schulson, E. M. and P. Duval, 2009. Creep and fracture of ice, Cambridge university press, chap. Elasticity, friction and diffusivity, 62 – 63.

Stern, H. L. and R. W. Lindsay, 2009. Spatial scaling of Arctic sea ice deformaton, *J. Geophys. Res.*, **114**(C10017).

Thomas, D., 1999. The quality of sea ice velocity estimates, *J. Geophys. Res.*, **104**, 13627 – 13652.

Thorndike, A.S. and R. Colony, 1982. Sea ice motion in response to geostrophic winds, *J. Geophys. Res.*, **87**, 5845 – 5852.

Weiss, J., 2008. Intermittency of principal stress directions within Arctic sea ice, *Physical Review E*, **77**(056106).

Weiss, J., D. Marsan and P. Rampal, 2009. Space and time scaling laws induced by the multiscale fracturing of the Arctic sea ice cover, Springer (P. Borodich Ed.), 101 – 109.

Weiss, J. and E.M. Schulson, 2009. Coulombic faulting from the grain scale to the geophysical scale: lessons from ice, *J. Phys. D: Appl. Phys.*, **42**(214017).

Weiss, J., E.M. Schulson and H.L. Stern, 2007. Sea ice rheology from in-situ, satellite and laboratory observations: Fracture and friction, *Earth Planet. Sci. Lett.*, **255**, 1 – 8.

Symbol	Meaning	Value
h	Ice thickness	
c	Ice concentration	
K	Effective elastic Modulus	
Y	Young Modulus	500 MPa
ν	Stiffness / Ice strength constant	20
d_0	Damage parameter	0.85
τ	Shear stress	
σ_N	Normal stress	
μ	Internal friction coefficient	0.7
C	Cohesion	10 to 20 kPa
$\sigma_{tension}$	Tensile strength	−40 kPa
ρ_a	air density	1.3 kg.m^{-3}
C_a	air drag coefficient	0.0012
u_{10}, v_{10}	10m wind speed	
ρ_w	water density	1025 kg.m^{-3}
C_w	water drag coefficient	0.0055
e	Ellipse aspect ratio (VP)	2
γ_{min}	Minimum plastic deformation rate (VP)	$10^{-9}s^{-1}$
P^*	Ice strength parameter (VP)	2.10^4 Nm^{-2}

Table 1. Physical parameters and constants

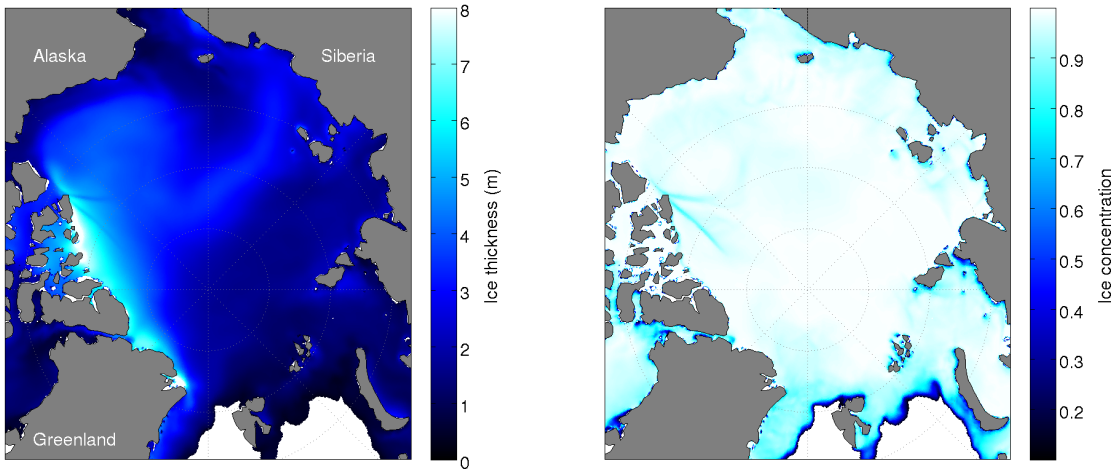

Fig. 1. Initial conditions of ice thickness and concentration for the simulations, extracted from the Drakkar ORCA025-G70 simulation

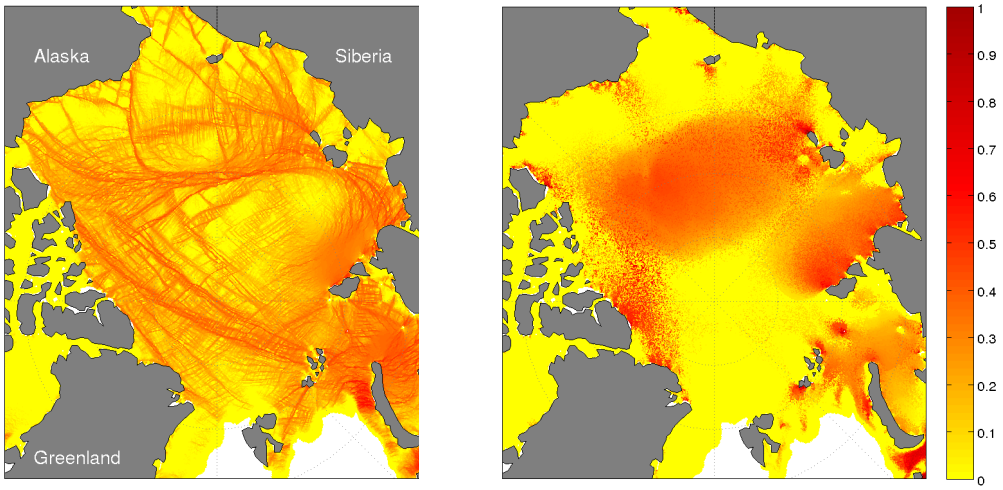

Fig. 2. Normalized number of damage events at the end of an EB-simulation. The left panel shows the normal result, where damage events induce a progressive reduction of the elastic modulus. On the right panel the reduction of elastic modulus has been desactivated ($d_0 = 1$), damage events are thus not followed by stress relaxation. The difference between the two fields illustrates the importance of elastic interactions (simulation start date is 2007-March-27).

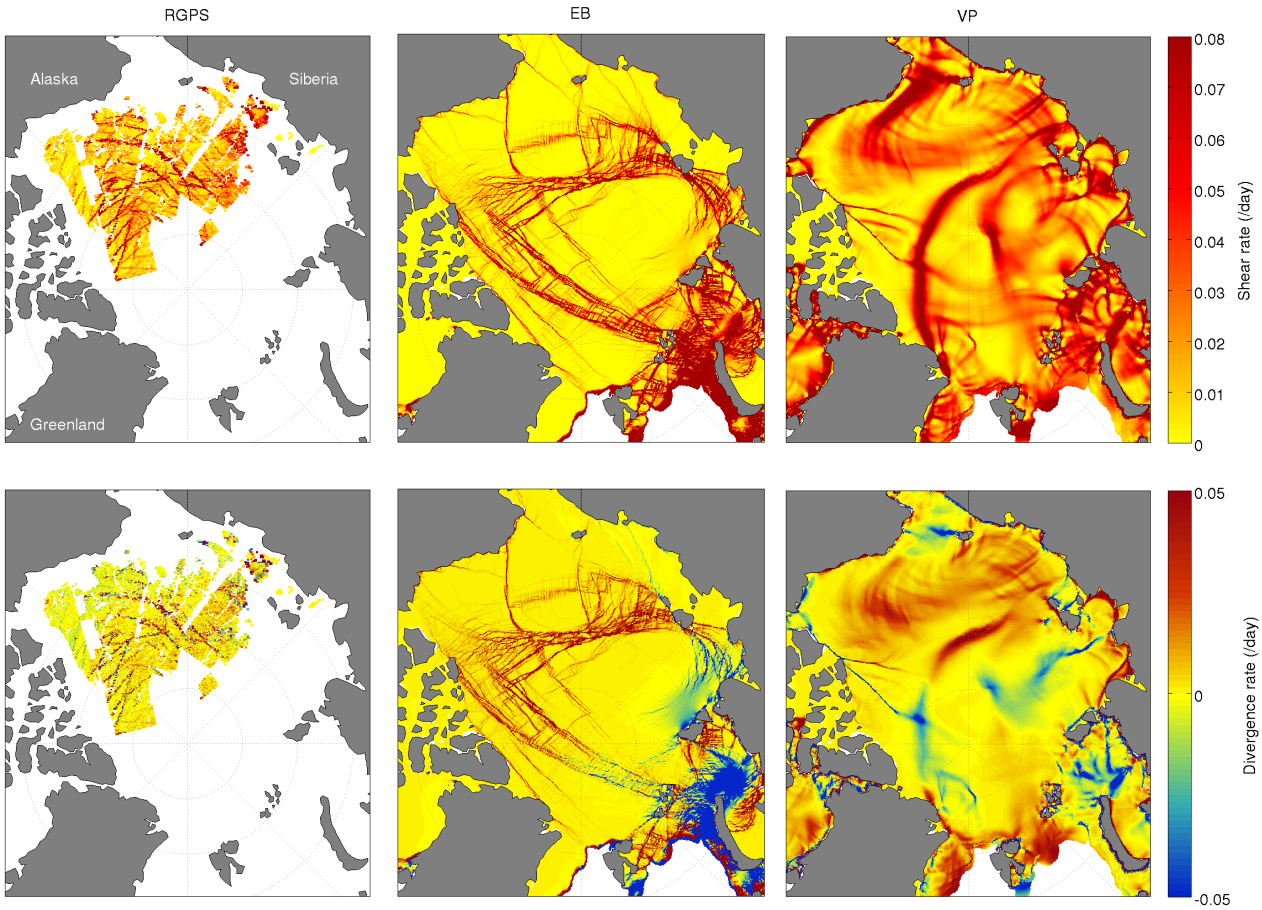

Fig. 3. Shear and divergence rate (/day) for 2007-March-27 from RGPS observations (1^{st} column), EB simulation (2^{nd} column) and VP simulation (3^{rd} column), calculated for a temporal scale of 3 days.

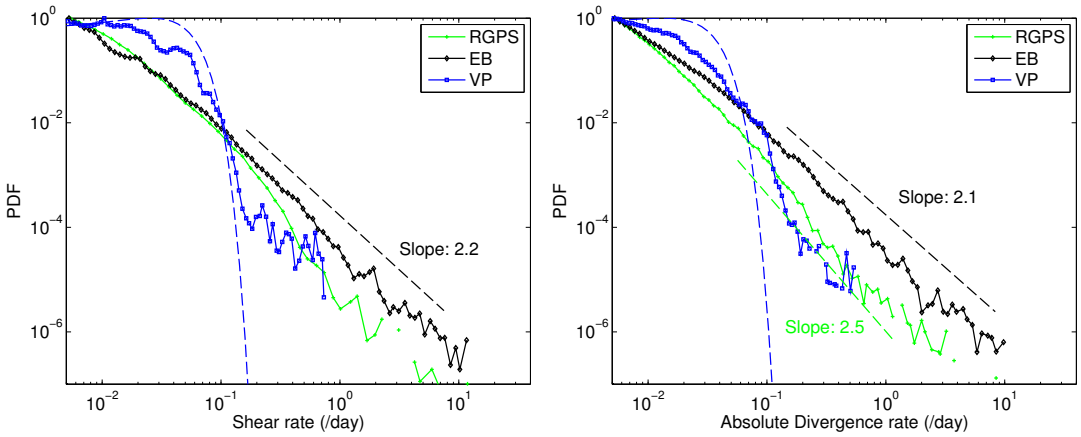

Fig. 4. PDF of shear and absolute divergence rate (/day) for EB simulation, VP simulation and RGPS observations. The strain-rate are calculated at the spatial scale of 10 km and temporal scale of 3 days. For RGPS and EB, dashed lines indicate the exponents of power law tails, the blue dashed line is the gaussian distribution of same mean and standard deviation as the VP distribution. PDFs are normalized by their maximal value.

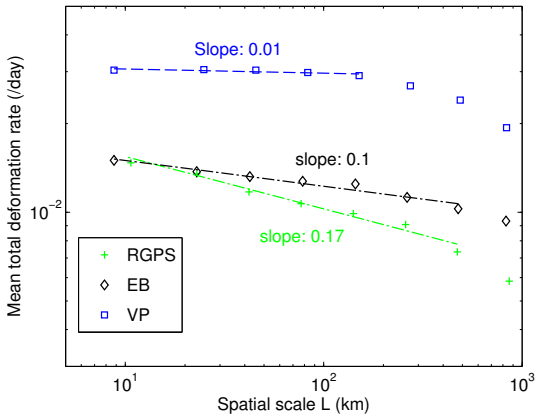

Fig. 5. Mean total deformation rate (/day) as a function of the spatial scale L. The dashed lines are power law fits to the data.